Beyond the harmonic bending theory of ionic surfactant interfaces

A. Fogden,[1,2] I. Carlsson,[1] and J. Daicic[2,3]
[1]*Physical Chemistry 1, Center for Chemistry and Chemical Engineering, University of Lund, Box 124, 22100 Lund, Sweden*
[2]*Department of Applied Mathematics, Research School of Physical Sciences and Engineering, Canberra, Australian Capital Territory 0200, Australia*
[3]*Institute for Surface Chemistry, Box 5607, 11486 Stockholm, Sweden*
(Received 5 December 1997)

There is now a broad understanding of how electrostatics, described by the nonlinear Poisson-Boltzmann equation, contributes to the phenomenological coupling (bending) constants of the flexible surface model as applied to ionic surfactant interfaces when the curvature energy density is truncated at harmonic order. Here, we extend this to the constants associated with anharmonic terms, specifically at third order in the interfacial curvatures, using model aggregates of spherical and cylindrical geometry. We analyze in detail the two limits of excess added salt and counterions only, and also provide a simple construction for bridging these two extremes using the theory of θ functions. Further, we investigate the asymptotic nature of the curvature expansion for ionic membranes, showing that it progressively deteriorates as the aggregate curvature is increased, and offer an alternative approximation scheme for the full free energy, using the method of Padé approximants. [S1063-651X(98)00405-X]

PACS number(s): 68.10.Et, 82.65.Dp, 62.20.Dc

I. INTRODUCTION

The flexible surface model of surfactant interfaces [1] provides a useful phenomenological tool for the understanding of mesophases formed by amphiphilic molecules in solution. As a phenomenological theory, it offers insight into the physics of these systems by subsuming a great deal of molecular detail (both in terms of structure and interactions) into its parameters. The aim of expressing these parameters in terms of molecular quantities stems from a natural desire to understand physical systems from a fundamental perspective, and also to allow a correspondence to experimental variables (e.g., composition, temperature) to be made.

This goal has, in part, been achieved for ionic surfactant systems. Expansions of the Poisson-Boltzmann (PB) equation, a mean-field description of electrostatic interactions for systems with charged interfaces and ions in solution, have allowed the incorporation of electrostatic effects into the curvature description [2–16]. Rather than give a detailed overview here, we refer the reader to reviews as given in Ref. [17] and the Introduction of Ref. [13]. Suffice it to say that within the PB description, we now understand how the bending rigidity k_c, saddle-splay modulus $\bar{k}_c$, and the product $k_c H_0$, where H_0 is the membrane spontaneous curvature, behave as functions of salt and surfactant concentration, and the surface charge density of the interfacial film.

The three bending ''constants'' just described are the coupling constants associated with an expansion of the curvature free energy density to harmonic (second) order. While this has been considered an adequate description for many systems, the relative stability of certain phases, such as the bicontinuous cubics [18], sponges and bicontinuous microemulsions [19], and lamellar phases with passage defects [11], requires the extension of the scheme to higher orders, an issue first considered by Mitov [20]. In a recent review, Morse [21] has underscored the role of anharmonic contributions in lifting the degeneracy of the harmonic bending energies for such phases. In this context, it is important in our view to find definitive criteria as to when the truncated curvature expansion fails to remain an adequate approximation to the full system free energy, and indeed to resolve whether or not the addition of the first anharmonic correction terms actually improves the situation significantly. The resolution of this issue hinges fundamentally on the asymptotic nature of the expansion. Thus the general aim is to test the validity of the commonly used curvature description, and to suggest ways of extending the range of its applicability where possible.

The study most closely related to the present one is contained in Ref. [15], which employs an undulating planar geometry to deduce the electrostatic contribution to moduli associated with fourth-order terms. Also, McAvity [10] has calculated the third-order moduli in the limit of low surface charge density, where the PB equation can be linearized, using a general surface deformation, and de Vries [11] derived scaling laws for one of the fourth-order moduli (that associated with the square of the Gaussian curvature). All of these studies, while extending the traditional curvature expansion to anharmonic terms, have been restricted to the extreme of excess electrolyte (i.e., effectively isolated interfaces). In the current study we seek to carry this same extension in geometrical order across the full regime of system composition (i.e., confinement).

To this end, we present herein several developments. First, we consider PB cell models of spherical and cylindrical aggregates, and deduce the electrostatic contribution to the moduli associated with third order in the (monolayer) film curvatures. These contributions are derived without any limiting assumptions as to the composition, and are expressed in a compact integral form. We then give explicit analytical expressions for all moduli, up to third order, at the two extremes of salt concentration, namely, excess salt and counterions only. Moreover, we present a method, based on

the theory of θ functions, for developing the general formulas about these two limiting cases, providing greatly simplified, yet highly accurate, approximations spanning all intermediate salt concentrations. This technique, which significantly reduces the computational difficulties in modeling ionic surfactant phases, is illustrated with the formulas for the harmonic-order moduli.

To probe the validity of the curvature expansion (at least as regards the electrostatic contributions) at the second and third orders, we compare its predictions with the exact numerical solutions for the PB cell models. The comparison clearly demonstrates that, as the monolayer radius of curvature is decreased (e.g., to around the Debye screening length in the case of excess salt), the harmonic truncation ceases to remain a faithful representation of the free energy. Furthermore, the improvement given by adding anharmonic corrections eventually leads to even greater spurious divergences at these high curvatures. This is to be expected; however, here we will provide an alternative scheme which may, in some cases, offer a remedy: the curvature expansion can be recast, using the method of Padé approximants, to provide a good approximation to the full electrostatic free energy over a much broader range of curvatures.

II. BENDING ENERGY AND ELECTROSTATIC FREE ENERGY

We begin with the classical Helfrich Hamiltonian [1], where the local curvature energy per unit area of interfacial surface, g_c, expanded to harmonic order, is given by

$$g_c = 2k_c(H-H_0)^2 + \bar{k}_c K, \tag{1}$$

where $H=(1/R_1+1/R_2)/2$ and $K=1/(R_1R_2)$ and R_1, R_2 are the two principal radii of curvature of the interface.

We consider adding to this second-order description the next- (i.e., third-) order corrections derived by Mitov [20]. In general, there are three such geometrical invariants at third order: the mean and Gaussian curvature products H^3 and HK, together with the surface Laplacian of H, leading to the combination

$$\lambda_1 H^3 + \lambda_2 HK + \lambda_3 \nabla^\nu \nabla_\nu H. \tag{2}$$

Here ∇ denotes the covariant differentiation given by the surface metric [22]. In this paper we shall focus on the first two of the three terms in Eq. (2). The Laplacian term can, in precisely the same manner as the saddle-splay term in Eq. (1), be reduced to a contour integral around the boundary of the surface via the divergence theorem. Accordingly, it does not enter into consideration for many geometries of interest, most importantly the cylindrical and spherical geometries which we shall address here. Combining Eqs. (1) and (2), the curvature free energy expansion up to third order for the cylinder and sphere of radius R gives, on differentiation with respect to $1/R$,

$$\Delta_c \equiv \frac{\partial g_c}{\partial(1/R)} = -2k_cH_0 + k_c\frac{1}{R} + \frac{3}{8}\lambda_1\frac{1}{R^2}, \tag{3a}$$

$$\Delta_c \equiv \frac{\partial g_c}{\partial(1/R)} = -4k_cH_0 + 2(2k_c+\bar{k}_c)\frac{1}{R} + 3(\lambda_1+\lambda_2)\frac{1}{R^2}, \tag{3b}$$

respectively.

In the cell model, the system of ionic surfactant, 1:1 electrolyte and oil, is divided into identical cells, of either cylindrical or spherical geometry. Each cell has a hydrocarbon core sheathed with a surfactant monolayer, the charged groups of which are idealized as a uniform surface charge density $-\sigma$ at radius R. The surrounding electrolyte is confined by a concentric neutral boundary at radius $R+d$. Assuming a Boltzmann distribution of both counterions $(+e)$ and coions $(-e)$, the electrostatic potential ψ in $R \leqslant r \leqslant R+d$ must satisfy the Poisson-Boltzmann equation

$$\frac{d^2\psi}{dr^2} + \frac{\chi}{r}\frac{d\psi}{dr} = \frac{4\pi e}{\varepsilon}[n_-^c \exp(\beta e\psi) - n_+^c \exp(-\beta e\psi)], \tag{4}$$

where $\chi=1$ for cylinders and $\chi=2$ for spheres. The boundary conditions are

$$\frac{d\psi}{dr} = \frac{4\pi\sigma}{\varepsilon} \quad \text{at } r=R, \tag{5a}$$

$$\psi, \frac{d\psi}{dr} = 0 \quad \text{at } r=R+d. \tag{5b}$$

The coefficients $n_\pm^c$ in Eq. (4) are the number densities of counterions and coions at the cell boundary, and relate to the chemical potentials of salt (μ_s) and water (μ_w).

For comparison with Eq. (3) we require the electrostatic free energy per unit area of charged surface, $g_{\rm el}$, and in particular its variation with R at fixed total area. In a previous study [13] we derived the following convenient expression for the derivative with respect to $1/R$:

$$\Delta_{\rm el} \equiv \frac{\partial g_{\rm el}}{\partial(1/R)} = \frac{\chi}{1+\chi}\frac{\varepsilon}{4\pi}R\int_R^{R+d} dr\left[\frac{R}{r} - \left(\frac{r}{R}\right)^\chi\right]\left(\frac{d\psi}{dr}\right)^2, \tag{6}$$

which we shall make use of again here. With varying R we maintain a fixed σ value and are free to impose a further two constraints on the R dependence of the parameters $n_\pm^c$ and d. In Ref. [13], we addressed three scenarios of physical relevance. In the first case the chemical potentials μ_s and μ_w were both fixed, and accordingly the total amounts of salt (N_s) and water (N_w) could vary. The other two cases were fixed μ_s and N_w, and fixed N_s and N_w. In the present work we focus on the first case, and thus fix $n_\pm^c$ on varying R.

Although Eq. (6) only explicitly involves the electric field, it still requires the solution of the nonlinear PB equation (4). This cannot be obtained analytically for finite R, except for the special situation of the cylindrical geometry with no added salt $(n_-^c=0)$. In the following section we assume that R is sufficiently large that the equation can be developed in powers of $1/R$ about the planar state $(R=\infty)$. Comparison with Eq. (3) for the two geometries then permits identification of the electrostatic contribution to the general

elastic constants k_cH_0, k_c, $\overline{k_c}$, λ_1, and λ_2 of the curvature expansion of Eqs. (1) and (2). We then solve Eq. (4) numerically at finite R to compare the exact values of the derivative in Eq. (6) with the asymptotic expansion. This allows us to make conclusions, within the cell model, as to the range of R values over which each successive order of the asymptotic expansion gives an accurate and useful approximation.

III. EVALUATION OF THE MODULI

A. Curvature expansion

In the planar reference state, denote the corresponding values of $n_{\pm}^c$ and d as $n_{\pm,0}^c$ and d_0. We use the planar boundary value of the counterion number density to define a length

$$\lambda_D=\left(\frac{\varepsilon}{2\pi n_{+,0}^c\beta e^2}\right)^{1/2}. \tag{7}$$

This length is then used to scale distance from the charged surface, $x=(r-R)/\lambda_D$, and the cell thickness, $D=d/\lambda_D$, in both the cylindrical and spherical geometries, which we then expand in ascending powers of λ_D/R. So we write $n_{\pm}^c=\Sigma_{i=0}^{\infty}n_{\pm,i}^c(\lambda_D/R)^i$ and $D=\Sigma_{i=0}^{\infty}D_i(\lambda_D/R)^i$, where $D_i=d_i/\lambda_D$. We then seek the corresponding developments of the reduced potential $\phi=\beta e\psi$, i.e., the coefficients ϕ_i. In particular, we need to expand to second order ($i=0,1,2$) to determine the set of elastic constants k_cH_0, k_c, $\overline{k_c}$, λ_1, λ_2.

The reduced potential for the plane, ϕ_0, satisfies the differential equation

$$\phi_0''=2[\alpha_0\ \exp(\phi_0)-\ \exp(-\phi_0)], \tag{8}$$

where the prime denotes d/dx. Here we have introduced the ratio $\alpha_0=n_{-,0}^c/n_{+,0}^c$ which ranges from 0 (for counterions only) to 1 (for excess salt). The solution of Eq. (8) gives elliptic integrals of the first kind F:

$$x=F(\theta_0,\alpha_0^{1/2})-F(\theta_0^s,\alpha_0^{1/2}), \tag{9}$$

where $\exp(\phi_0/2)=\sin\theta_0$ and θ_0^s is the value of θ_0 at the charged surface. Inverting this relation gives $\phi_0(x)$ as the logarithm of a Jacobi elliptic function, with the scaling length λ_D given by the boundary condition (5a):

$$\frac{\lambda_D}{\lambda_{GC}}=\cot\theta_0^s(1-\alpha_0\ \sin^2\theta_0^s)^{1/2}. \tag{10}$$

Here, we have absorbed the (conserved) value of σ into the Gouy-Chapman length $\lambda_{GC}=\varepsilon/(2\pi\beta e\sigma)$. The pair of parameters α_0 and θ_0^s carried in Eqs. (9) and (10) may be readily eliminated in terms of the relevant pair of system properties (mentioned above) to be conserved on bending.

We then perform the perturbation of the differential equation (4) together with the boundary conditions (5) to obtain the next two corrections $\phi_1(x)$ and $\phi_2(x)$ for both $\chi=1$ (cylinder) and $\chi=2$ (sphere) in terms of this planar solution. For the case of conservation of μ_s and μ_w (so $n_{\pm,1}^c=n_{\pm,2}^c=0$) ϕ_1 must satisfy the differential equation

$$\phi_1''-2[\alpha_0\ \exp(\phi_0)+\exp(-\phi_0)]\phi_1=-\chi\phi_0' \tag{11}$$

and ϕ_2 is in turn a solution of

$$\phi_2''-2[\alpha_0\ \exp(\phi_0)+\exp(-\phi_0)]\phi_2=-\chi\phi_1'+\chi x\phi_0'+\frac{1}{2}\phi_0''\phi_1^2. \tag{12}$$

The perturbation in the potential is then inserted into Eq. (6) to provide the corresponding development of Δ_{el} in powers $(\lambda_D/R)^i$. The coefficients for $i=0$ and 1 were derived in the previous study [13], while that for $i=2$ is given by

$$-\frac{\varepsilon}{4\pi(\beta e)^2}\int_0^{D_0}dx\ x\left[2\chi\phi_0'\phi_2'+\chi(\phi_1')^2+(\chi-2)x\phi_0'\phi_1'+\frac{\chi}{\chi+1}x^2(\phi_0')^2\right]. \tag{13}$$

The elimination of ϕ_1 and ϕ_2 from Eq. (13) follows from the same procedure as was used previously and will not be detailed here. Suffice it to say that the manipulation at this higher order is considerably more involved but again only relies upon the defining differential equations (11) and (12) and not their explicit solutions. This elimination from Eq. (13) gives, both for cylinders and spheres, a simplified form for the coefficient which, like those for $i=0$ and 1, contains only the derivatives of ϕ_0 and in particular, moments of the square of the electric field for the plane

$$\mathcal{E}^{(j)}(x)=\int_x^{D_0}dx\ x^j(\phi_0')^2. \tag{14}$$

B. Expressions at general system composition

In the previous study [13] we showed that

$$k_cH_0=\frac{\varepsilon}{8\pi(\beta e)^2}\mathcal{E}^{(1)}(0) \tag{15}$$

and

$$\overline{k_c}=-\frac{\varepsilon\lambda_D}{4\pi(\beta e)^2}\mathcal{E}^{(2)}(0). \tag{16}$$

Moreover, the dependence of $\phi_1(x)$ on the particular choice of closure constraint canceled from Eq. (16), thus verifying the general predictions of the pressure-profile approach [13]. The formula for k_c does, however, depend on which of the three constraints is imposed. For the case of fixed μ_s and μ_w, we found that

$$k_c=\frac{\varepsilon\lambda_D}{4\pi(\beta e)^2}\int_0^{D_0}dx\ (\phi_0')^{-1}\frac{d}{dx}[(\mathcal{E}^{(0)})^2/\phi_0'']. \tag{17}$$

The electrostatic contribution to the third-order modulus λ_1 is obtained by equating the simplified form of Eq. (13) for $\chi=1$ with the coefficient $\frac{3}{8}\lambda_1/\lambda_D^2$ from the curvature free energy expansion Eq. (3a). Its partner λ_2 is then isolated by equating the simplification of Eq. (13) for $\chi=2$ to the coefficient $3(\lambda_1+\lambda_2)/\lambda_D^2$ from Eq. (3b). The final formula for λ_1 is

$$\lambda_1 = -\frac{\varepsilon\lambda_D^2}{\pi(\beta e)^2}\Bigg\{(\mathcal{E}^{(0)}/\phi_0'')^2+\frac{1}{3}[\phi_0'\phi_0'''-(\phi_0'')^2] \times[\mathcal{E}^{(0)}/(\phi_0'\phi_0'')]^3+\int_0^{D_0}dx\; x(\mathcal{E}^{(0)}/\phi_0')^2 + \int_0^{D_0}dx\;(\mathcal{E}^{(0)})^3/(\phi_0')^4\Bigg\}. \tag{18}$$

Note that in the first two of the four terms, all $\mathcal{E}^{(0)}$ and derivatives of ϕ_0 should be evaluated at the charged surface $x=0$. For λ_2 we obtain

$$\lambda_2=\frac{\varepsilon\lambda_D^2}{\pi(\beta e)^2}\int_0^{D_0}dx\;(\phi_0')^{-1}\frac{d}{dx}(\mathcal{E}^{(0)}\mathcal{E}^{(1)}/\phi_0''). \tag{19}$$

The formulas in Eqs. (15)–(19) are general in the sense that no limitations have been imposed on the parameters α_0 and θ_0^s characterizing the planar-state solution in Eqs. (9) and (10) [23]. In Ref. [13] we inserted ϕ_0 into Eqs. (15)–(17) and integrated numerically to generate the values of these electrostatic contributions to k_cH_0, $\overline{k_c}$, and k_c for typical ranges of added salt concentration, surfactant volume fraction, and headgroup area. Values for the corresponding contributions to the third-order moduli λ_1 and λ_2 can similarly be obtained in a straightforward manner from Eqs. (18) and (19), albeit with the restriction to the case of fixed μ_s and μ_w. However, in this study we shall focus on the two extremes of electrostatic screening, namely, the situations in which salt is either present in excess ($\alpha_0=1$) or absent altogether ($\alpha_0=0$), while maintaining an arbitrary θ_0^s. These two extremes are often experimentally relevant and well describe the general trends, with the advantage of yielding compact analytic formulas for the moduli. Most importantly, these two end points of the α_0 range admit analytic developments which, owing to their rapid convergence, can be regarded as essentially exact forms even at the lowest levels of truncation.

C. Excess salt

In this extreme the surfactant aggregate is effectively isolated, i.e., the cell thickness d_0 is infinite and the number densities $n_{\pm,0}^c$ at the cell boundary take on the bulk number density n_B of the 1:1 electrolyte. Accordingly, all three cases of constraints on μ_s, μ_w, N_s, N_w mentioned above become identical. It is now more convenient to switch from λ_D in Eq. (7) to a scaling length equal to one-half of this, the standard Debye screening length

$$\kappa^{-1}=\left(\frac{\varepsilon}{8\pi n_B\beta e^2}\right)^{1/2}. \tag{20}$$

The moduli are then functions of the single variable κ^{-1}/λ_{GC}, aside from the dimensioned factor $\varepsilon/[\pi(\beta e)^2]\kappa^{-(m-1)}$ multiplying each, where m is the order of the curvature free energy term (i.e., $m=1$ for k_cH_0, $m=2$ for k_c and $\overline{k_c}$ and $m=3$ for λ_1 and λ_2).

The formulas for the general third-order moduli in Eqs. (18) and (19) in this excess-salt limit are given in Appendix A, where we also provide the previously established results for k_cH_0, $\overline{k_c}$, and k_c. In addition, we have included there the corresponding formula for the modulus of one of the fourth-order terms in the curvature free energy expansion. At fourth order eight independent terms enter g_c, although for cylindrical or spherical geometries these reduce to the three products of H and K [20],

$$16\kappa_1H^4+4\kappa_2H^2K+\kappa_3K^2. \tag{21}$$

Further, the latter two vanish for the cylinder so the next-order correction to Eq. (3a) is just $4\kappa_1/R^3$. The formula for this modulus κ_1 is given in Eq. (A8) and was obtained by analyzing the anharmonic undulations of an isolated charged sheet [15]. We shall consider the effect of this extra correction in subsequent sections, however we shall not go beyond third order for the sphere. Note that the formulas (A1)–(A8) pertain to an arbitrary value of the ratio κ^{-1}/λ_{GC}.

If the surface is weakly charged and/or highly screened (so that $\kappa^{-1}/\lambda_{GC}\ll 1$) then all of the moduli in Eqs. (A3)–(A8) vanish according to the asymptotic form

$$C\frac{\varepsilon}{\pi(\beta e)^2}\frac{\kappa^{-(m+1)}}{\lambda_{GC}^2}, \tag{22}$$

where C is a number and m is again the order of the expansion. The values of C for k_cH_0, k_c, $\overline{k_c}$, λ_1, λ_2, and κ_1 are 1/8, 3/8, $-1/4$, $-3/2$, 1, and 63/256, respectively. In particular, these scaling forms for λ_1 and λ_2 agree precisely with the conclusions of McAvity [10]. In this low charge limit the PB equation can be linearized and Eq. (6) can be evaluated for an arbitrary radius R. For the sphere this gives the simple Debye-Hückel result

$$\Delta_{el}=-\frac{\varepsilon}{2\pi(\beta e)^2}\left(\frac{\kappa^{-1}}{\lambda_{GC}}\right)^2\left(1+\frac{1}{\kappa R}\right)^{-2} \tag{23}$$

while for the cylinder

$$\Delta_{el}=-\frac{\varepsilon}{2\pi(\beta e)^2}\left(\frac{\kappa^{-1}}{\lambda_{GC}}\right)^2\Bigg\{(\kappa R)^2\left(\left[\frac{K_0(\kappa R)}{K_1(\kappa R)}\right]^2-1\right) + \kappa R\frac{K_0(\kappa R)}{K_1(\kappa R)}\Bigg\}, \tag{24}$$

where K_0 and K_1 are the modified Bessel functions of the second kind of orders 0 and 1. Expansion of the solutions in powers of κ^{-1}/R and matching to Eq. (3) duly restores the above results for the coefficients C of these moduli and indeed can be trivially extended to higher orders. For the sphere the coefficient of $1/R^{m-1}$, $m\geq 1$, in Eq. (23) is given by Eq. (22) with $C=(-1)^m m/2$, so, in particular, $C=1/2$ for the combination $16\kappa_1+4\kappa_2+\kappa_3$ in Eq. (21). In the cylindrical geometry, Eq. (24), the general formula for the C corresponding to the power $1/R^{m-1}$ is more complicated, but the first few values can be calculated in a straightforward manner; we find that $C=-1/4$, 3/8, $-9/16$, 63/64, and $-135/64$ for $m=1$ to 5, respectively.

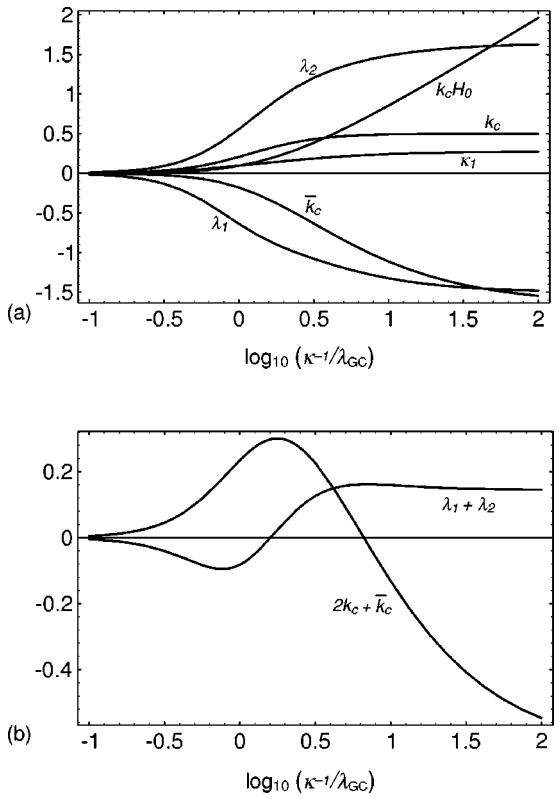

FIG. 1. Plots of (a) the six individual moduli considered in this study, and (b) the two combined coefficients in spherical geometry, for the case of salt in excess, ranging from low to high surface charge. The common prefactor (given in the text) has been removed from each.

In the opposite limit of high charge and weak screening (so that $\kappa^{-1}/\lambda_{GC} \gg 1$ and the PB equation cannot be linearized), all of the moduli diverge. The first-order modulus k_cH_0 diverges logarithmically,

$$k_cH_0 \sim \frac{\varepsilon}{2\pi(\beta e)^2} \ln(\kappa^{-1}/\lambda_{GC}), \tag{25}$$

and the higher-order ($m \geqslant 2$) coefficients follow the power-law form

$$C' \frac{\varepsilon}{\pi(\beta e)^2} \kappa^{-(m-1)}. \tag{26}$$

Here the value of the numerical factor C' for k_c, $\bar{k}_c$, λ_1, λ_2, and κ_1 is 1/2, $-\pi^2/6$, $-3/2$, $\pi^2/6$, and 53/192, respectively.

In Fig. 1(a) the six moduli in Eqs. (A3)–(A8) are plotted over a broad range of κ^{-1}/λ_{GC} on a logarithmic scale (with their dimensioned prefactors $\varepsilon/[\pi(\beta e)^2]\kappa^{-(m-1)}$ removed for comparison). The moduli all maintain the same sign throughout and monotonically increase in magnitude. By virtue of the common power laws in Eqs. (22) and (26), the dimensionless ratios $\lambda_1\kappa/k_c$, $\lambda_2\kappa/k_c$, and $\kappa_1\kappa^2/k_c$ do not vary markedly across this entire range, e.g., $\lambda_2\kappa/k_c$ rises from 2.67 up to only 3.29. In Fig. 1(b) we plot the particular combinations $2k_c+\bar{k}_c$ and $\lambda_1+\lambda_2$ (again rendered dimensionless by omission of the prefactor mentioned above) which enter into the sphere expansion in Eq. (3b). In contrast to the individual moduli, and hence to the cylinder expansion, these combinations change sign and are nonmonotonic. The dimensionless $2k_c+\bar{k}_c$ has a maximum of 0.301 at $\kappa^{-1}/\lambda_{GC}=1.77$ and changes sign at 6.64. The corresponding third-order sum $\lambda_1+\lambda_2$ reaches a minimum of -0.095 at $\kappa^{-1}/\lambda_{GC}=0.765$, crosses the axis at 1.60, and attains its maximum of 0.162 at 7.04. Thus for the sphere up to third order, the range κ^{-1}/λ_{GC} divides into three intervals. As κ^{-1}/λ_{GC} increases beyond 1.60, Δ_{el} still increases from $1/R=0$ but switches from downward to upward curving, while beyond 6.64 it becomes decreasing from $1/R=0$.

In the second part of Appendix A we use these foregoing results as a basis for pseudo-closed formulas for the moduli at arbitrary composition in Sec. III B. These formulas serve to eradicate the unnecessary complications of integrating unwieldy elliptic functions, or resort to numerical methods. This broadly applicable analytical technique proceeds by replacing elliptic functions with θ functions, and accordingly rewrites the slowly convergent series in α_0 or $1-\alpha_0$ as powerfully converging expansions in the corresponding ''nome'' [24]. The fundamentals have been described in detail by Ninham and Parsegian [25] in the context of charge regulation models; here we furnish only the final expressions. Equations (A9)–(A15) give the harmonic moduli k_cH_0, $\bar{k}_c$, and k_c, truncated at the second power in the nome. These approximations remain extremely accurate from $\alpha_0=1$ down to below $\alpha_0=1/2$, thus spanning the majority of the parameter space from excess salt to counterions only.

D. Counterions only

In the absence of added salt there are no coions present, so that $n^c_{-,0}$, and α_0, are zero. For this extreme the constraints of fixed μ_s, N_w and fixed N_s, N_w become identical, but remain distinct from the case of fixed μ_s, μ_w which we consider here. Although the scaling length λ_D in Eq. (7) is now a natural analog of the excess-salt variable κ^{-1}, we shall use the planar cell width d_0 here and regard the moduli as functions of the ratio d_0/λ_{GC} with the dimensioned prefactor $\varepsilon/[\pi(\beta e)^2]d_0^{m-1}$. In the first part of Appendix B we evaluate λ_1 and λ_2 [Eqs. (18) and (19)] in the counterions-only regime, and also the corresponding expressions for k_cH_0, $\bar{k}_c$, and k_c [from Eqs. (15)–(17)] using the same notation.

Without added salt, the PB equation admits an analytic solution for cylindrical symmetry [26,14]

$$\frac{d\phi}{dr} = \frac{2}{r}\{1-\gamma \tan[\gamma \ln(r/r_0)]\}. \tag{27}$$

The boundary conditions (5) of the cylindrical cell model then determine the two parameters γ and r_0, and for the current case of fixed chemical potentials the thickness d is also specified as a function of R, λ_D, and λ_{GC}. In particular, eliminating r_0 and d, γ must satisfy the transcendental equation

$$\gamma \tan\left(\gamma \ln\left[\frac{\lambda_D}{R}(\gamma^2+1)^{1/2}\right]\right) = \frac{R}{\lambda_{GC}}\left(1-\frac{R}{\lambda_{GC}}\frac{1}{\gamma^2}+\frac{1}{\gamma^2}\right)^{-1}. \tag{28}$$

The derivative in Eq. (6) which we seek here is then given as

$$\Delta_{\rm el}=-\frac{\varepsilon}{4\pi(\beta e)^2}\left\{\gamma^2+1-\left(\frac{R}{\lambda_D}\right)^2 -2(\gamma^2-1)\,\ln\left[\frac{\lambda_D}{R}(\gamma^2+1)^{1/2}\right] +2\ln\left[\frac{\gamma^2+(R/\lambda_{\rm GC}-1)^2}{\gamma^2+1}\right]\right\}. \tag{29}$$

We now introduce the assumption of large R/λ_D and determine the coefficients of the perturbation $\gamma=(\lambda_D/R)^{-1}+\Sigma_{i=0}^{\infty}\gamma_i(\lambda_D/R)^i$ which meet Eq. (28) at each order. Inserting this perturbation into Eq. (29) and expanding, the resulting terms for $i=0$, 1, and 2 match precisely the prescription in Eq. (3a) using the formulas in Appendix B for k_cH_0, k_c, and λ_1, respectively. Further, if we proceed to $i=3$ and match the resulting coefficient of $1/R^3$ in Eq. (29) with the prescription $4\kappa_1$ from Eq. (21) then we obtain the electrostatic contribution to this fourth-order modulus κ_1. This formula is given as Eq. (B8), and thus provides the counterions-only analog of the excess salt result in Eq. (A8). Again, note that, as for excess salt, Eqs. (B1)–(B8) apply for all values of $d_0/\lambda_{\rm GC}$.

If the system is weakly charged ($d_0/\lambda_{\rm GC}\ll 1$), then the moduli in Eqs. (B3)–(B8) adopt the asymptotic forms

$$C\frac{\varepsilon}{\pi(\beta e)^2}\frac{d_0^{m+1}}{\lambda_{\rm GC}^2}. \tag{30}$$

The numerical factors C for the six moduli k_cH_0, k_c, $\overline{k_c}$, λ_1, λ_2, and κ_1 are 1/24, 2/15, $-1/30$, $-8/15$, 13/90, and 8/105, respectively. On the other hand, for highly charged surfaces ($d_0/\lambda_{\rm GC}\gg 1$) the first-order modulus k_cH_0 becomes logarithmic,

$$k_cH_0\sim\frac{\varepsilon}{2\pi(\beta e)^2}\ln(d_0/\lambda_{\rm GC}), \tag{31}$$

while the moduli for orders $m\geqslant 2$ follow the power law

$$C'\frac{\varepsilon}{\pi(\beta e)^2}d_0^{m-1}. \tag{32}$$

The values of C' for k_c, $\overline{k_c}$, λ_1, λ_2, and κ_1 are now 0.178, -0.564, -0.170, 0.183, and 0.0091. Note that the scalings (30)–(32) are identical to those for excess salt [Eqs. (22), (25), (26)] on interchange of d_0 and κ^{-1}, as expected from dimensionality.

Figure 2(a) displays the variation of the six moduli in Eqs. (B3)–(B8) between these two limits. The dimension factor $\varepsilon/[\pi(\beta e)^2]d_0^{m-1}$ has been divided out of each, and κ_1 multiplied by 16 [as it occurs in Eq. (21)] to become clearly visible on this common vertical scale. The moduli never change sign, but as opposed to Fig. 1(a) for excess salt, the transitions between the two limits are no longer strictly monotonic. The dimensionless k_c has a maximum of 0.181 at $d_0/\lambda_{\rm GC}=22.3$, while λ_1 passes through a very flat section

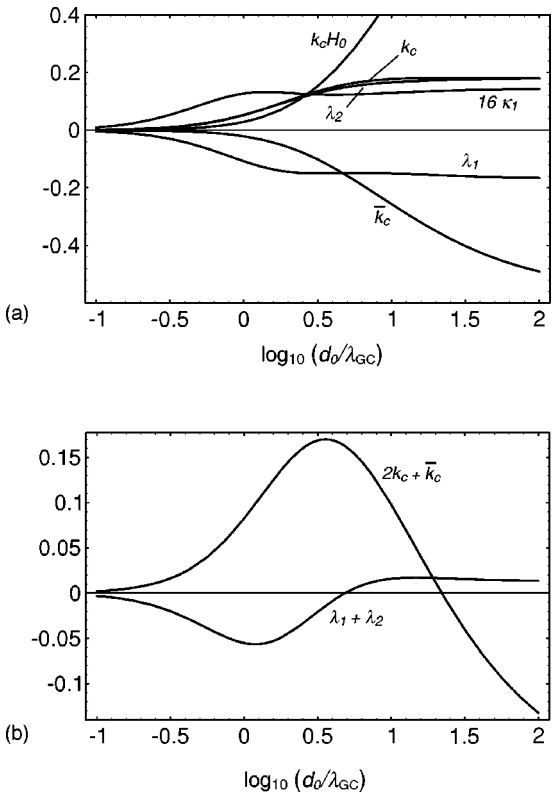

FIG. 2. Analog of Fig. 1 for the opposing extreme of counterions only, again ranging from weak to strong charge (the so-called ''ideal gas'' and ''Gouy-Chapman'' regimes, respectively).

from a minimum of -0.150 at $d_0/\lambda_{\rm GC}=3.18$ to a maximum of -0.148 at 6.19. Also $16\kappa_1$ reaches a maximum of 0.132 at 1.42 and passes through a minimum of 0.123 at 4.04. Note that the curves for the four positive moduli all intersect around $d_0/\lambda_{\rm GC}=2.5$ to 2.7. In particular, the pair of curves for k_c and λ_2 are almost superimposed throughout; the ratio $\lambda_2/(k_cd_0)$ only varies between 0.933 and 1.08. Figure 2(b) shows the variation in the second- and third-order combinations $2k_c+\overline{k_c}$ and $\lambda_1+\lambda_2$ (again in the same dimensionless form) for the sphere in Eq. (3b). The trends here are qualitatively identical to those in Fig. 1(b) for excess salt. The curve for $2k_c+\overline{k_c}$ has its maximum of 0.170 at $d_0/\lambda_{\rm GC}=3.58$ and crosses the axis at 22.1. The $\lambda_1+\lambda_2$ curve has its minimum of -0.056 at 1.20, changes sign at 4.84, and rises to its maximum value of 0.017 at 14.8. Accordingly, the behavior of $\Delta_{\rm el}$ local to $1/R=0$ follows the three-stage progression for excess salt.

Note that the ratio $-\overline{k_c}/k_c$, which dictates the stability within the harmonic bending energy description, is around 3.2 in the high charge limit (in which the electrostatics could be expected to dominate the intrinsic contributions to the moduli), both for excess salt and counterions only. Further, the ratio $-\lambda_2/\lambda_1$, providing its analog at third order, displays similar insensitivity at these two extremes, with a value around one-third of that for $-\overline{k_c}/k_c$.

In the second part of Appendix B the preceding analysis becomes the foundation for constructing simplified formulas for the bending moduli at arbitrary system composition, which complement the results in Appendix A. The θ function technique operates in a completely analogous manner

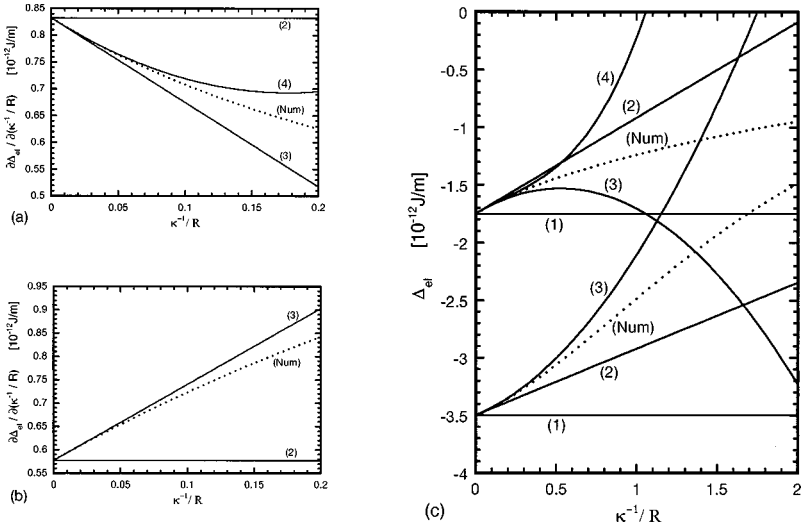

FIG. 3. PB cell models for 250 mM salt in excess, surrounding an ionic surfactant monolayer of headgroup area 67 Å^2, comparing the numerical solution with ascending orders of curvature expansion. Plots of the first derivative of Δ_{el} in Eq. (6) for (a) cylinders and (b) spheres, of relatively slight curvatures, together with (c) Δ_{el} across a broader range of cylinder (upper) and sphere (lower) curvatures. See the text for a detailed description.

about this opposing extreme; the final formulas for $k_c H_0$, $\overline{k_c}$, and k_c are given in Eqs. (B9)–(B13). These expansions, again truncated at the second power, suffice to maintain a very high accuracy from $\alpha_0=0$ to beyond $\alpha_0=1/2$. Thus, when taken together, the two developments bridge the full range of compositions and surface conditions. As one illustration of the utility of the formulas, in the highly charged limit ($t_p\to\infty$ and $z_0\to\pi/2$ in Appendixes A and B, respectively) the ratio $-\overline{k_c}/k_c$ is simply shown to monotonically increase with α_0 from counterions only to excess salt. So the abovementioned insensitivity of this stability ratio holds independently of the way in which the limits of vanishing surfactant volume fraction and electrolyte concentration are reached.

IV. COMPARISON WITH NUMERICAL SOLUTION

A. Curvature expansion

In this section, we shall consider particular charged systems and compare the exact free energy of their electrostatics with its contribution to the curvature free energy at the orders described in the preceding section. Since we have derived these contributions to the coefficients in Eqs. (1) and (2) (with the exception of λ_3) for an unspecified composition, we could in principle relate this to any interfacial configuration. However, we will limit our focus here to the cylindrical and spherical cells which gave rise to the moduli formulas, to avoid coupling the issue to the validity of these models for real configurations. Thus, for a given value of the radius R, we directly compare the Δ_{el} in Eq. (6), using the exact solution of the PB equation (4), with its asymptotic expansion in Eq. (3). Of course, for sufficiently small $1/R$ the curve of Δ_{el} will be approximated to increasing accuracy by the succession of terms in Eq. (3), i.e., the constant (from order $m=1$), the straight line ($m=2$), the parabola ($m=3$), and so on. However, as R is decreased the curvature approximation must eventually break down, with successive terms introducing an increasingly powerful divergence.

As in the preceding section we illustrate the behavior at a general composition by analyzing the two extremes of excess added salt and no added salt, addressing in particular the case of bending at fixed counterion chemical potential in the latter extreme. In doing so all formulas (A2)–(A8) and (B2)–(B8) will be used, giving developments of the sphere up to third order and the cylinder to fourth order by adding the $m=4$ term $4\kappa_1/R^3$ to Eq. (3a). To analyze in detail the deviation of the exact derivative Δ_{el} of g_{el} from its asymptotics at small $1/R$ it will also prove useful to take a second derivative, so the expansions in Eqs. (3a) and (3b) become

$$\frac{\partial\Delta_{el}}{\partial(1/R)}=k_c+\frac{3}{4}\lambda_1\frac{1}{R}+12\kappa_1\frac{1}{R^2}+\cdots, \tag{33a}$$

$$\frac{\partial\Delta_{el}}{\partial(1/R)}=2(2k_c+\overline{k_c})+6(\lambda_1+\lambda_2)\frac{1}{R}+\cdots \tag{33b}$$

for cylinders and spheres, respectively.

For excess salt, in the limit of small κ^{-1}/λ_{GC}, Δ_{el} was given by Eqs. (23) and (24) for spheres and cylinders, and comparison with their expansions, as discussed there, becomes a simple matter. In both geometries the coefficients of $1/R^{m-1}$ alternate in sign, however, the power series for the sphere has a radius of convergence $\kappa^{-1}/R=1$ while that for the cylinder is strictly asymptotic. Instead we shall focus on examples in which the nonlinearity is important, and we use a numerical procedure to generate the exact $(d\psi/dr)^2$ from Eq. (4) for Δ_{el} in Eq. (6). We consider two such scenarios, in both of which the area per charged surfactant headgroup is taken to be 67 Å^2 (and $T=298$ K for all examples here) so the Gouy-Chapman length $\lambda_{GC}=1.5$ Å. The bulk concentration of added salt is 250 mM in the first example and 10 mM in the second, so the Debye lengths κ^{-1} are 6.1 Å and 30 Å, respectively. The ratios κ^{-1}/λ_{GC} are 4.1 and 20, thus amounting to situations of moderate and weak screening. Recalling Fig. 1(b), which displays three regimes with increasing κ^{-1}/λ_{GC} based on the signs of the moduli combinations for the sphere, these two examples lie in the second and third regimes, respectively.

The results for these concentrations of 250 mM and 10 mM are summarized in Figs. 3 and 4, respectively. The parts (a) and (b) of both display the second derivative $\partial\Delta_{el}/\partial(1/R)$ for cylinders and spheres, respectively, of relatively large radius ranging from $R=\infty$ down to $R=5\kappa^{-1}$. The dotted curve (Num) is the exact numerical solution, while the solid

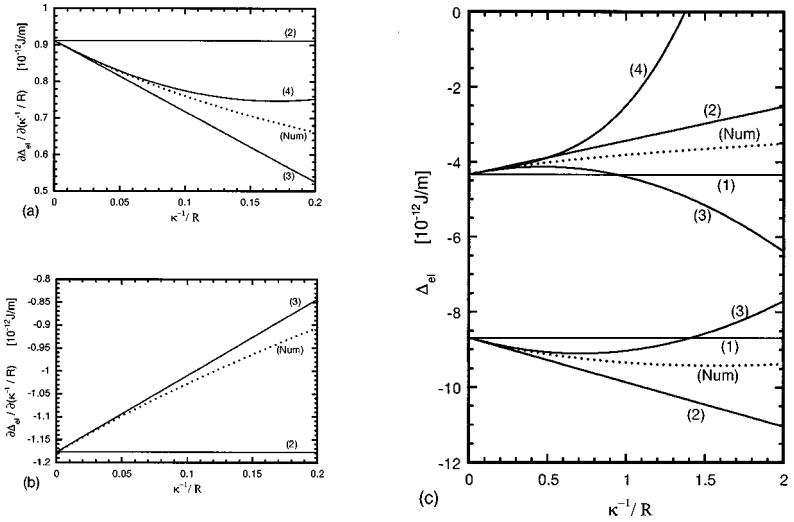

FIG. 4. The analog of Fig. 3 for 10 mM salt in excess, maintaining the headgroup area at 67 Å^2.

curves (m) are the asymptotic expansions in Eqs. (33) taken to curvature order m. For the sphere case (b) the constant $2(2k_c+\overline{k_c})$ in Eq. (33b) switches from positive to negative from Fig. 3 to 4 while the straight line slope $6(\lambda_1+\lambda_2)$ remains positive. Throughout this range of R values the curves for successive orders in m yield increasingly accurate approximations to the exact curves, however, the deviations grow rapidly with decreasing R. The errors associated with the highest orders, $m=4$ for the cylinder and 3 for the sphere, are all around 2% at $R=10\kappa^{-1}$ but have increased substantially at $R=5\kappa^{-1}$. Also note that for both concentrations the third-order expansion is a better approximation for the sphere (b) than for the cylinder (a). Although the plots in Figs. 3(a) and 4(a) appear very similar, as do their (b) counterparts, one must bear in mind that the κ^{-1} values used in their scalings differ by a factor of 5.

In Figs. 3(c) and 4(c) we plot the first derivative Δ_{el} (the cylinder is always above the sphere) from the planar limit down to $R=0.5\kappa^{-1}$, extending the range of κ^{-1}/R in (a) and (b) by an order of magnitude. The same labeling scheme applies, now with the solid curves (m) being the expansions to curvature order m in Eq. (3), also including the cubic polynomial for the cylinder to $m=4$. Out to $\kappa^{-1}/R=0.2$ the curves, which are difficult to distinguish, are just the integrals of those presented in parts (a) and (b). Note that the exact Δ_{el} for the sphere in Fig. 4(c) passes through a minimum, followed by an inflection point [as in Fig. 3(c)], on its way to approaching zero. The main feature of these plots is the increasingly dramatic deviations of successive orders of expansion as κ^{-1}/R rises to around order 1. Clearly the curvature expansions become completely inappropriate as approximations for this size of aggregate.

In the opposite extreme of no added salt we again consider two examples, in both of which the planar cell width d_0 (the half thickness of the water layer in a lamellar phase) is taken to be 50 Å. In the first example we assume one charge per 300 Å^2, which might represent a smeared-out model for a monolayer of nonionic surfactant containing some anionic surfactant. The Gouy-Chapman length is then 6.7 Å and the ratio $d_0/\lambda_{GC}=7.5$, so from Eq. (B2) $d_0/\lambda_D=1.39$. In the second example we return to the previous value of one charge per 67 Å^2, and so $d_0/\lambda_{GC}=34$ and thus $d_0/\lambda_D=1.53$. As for the excess-salt examples, these two d_0/λ_{GC} values lie in the second and third regimes of sign combinations for the sphere coefficients in Fig. 2(b). The results for the area per charge values of 300 Å^2 and 67 Å^2 are displayed in Figs. 5 and 6, respectively. These are plotted and labeled in exactly the same manner as for excess salt, with

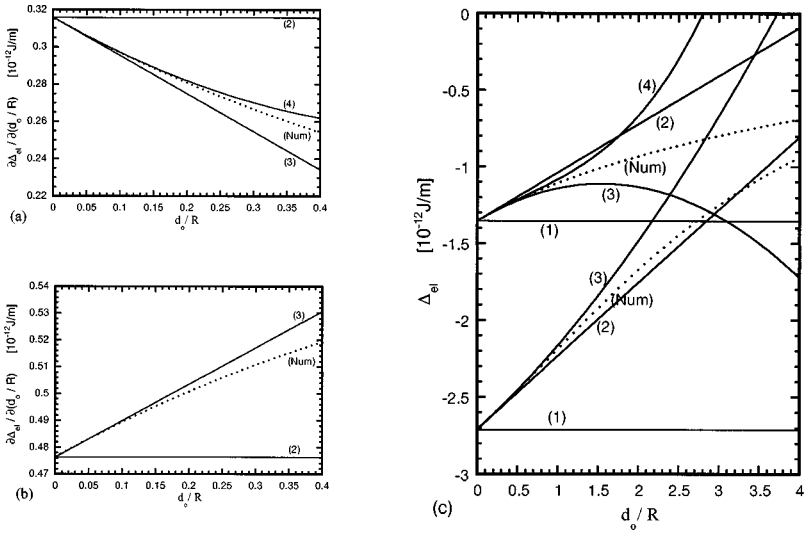

FIG. 5. PB cell models in the absence of electrolyte, with the surfactant monolayer (bearing one charge per 300 Å^2) surrounded by a corona of balancing counterions of thickness corresponding to $d_0=50$ Å in the planar reference state. The plots (a), (b), and (c) are as for Fig. 3, now replacing κ^{-1} by this d_0.

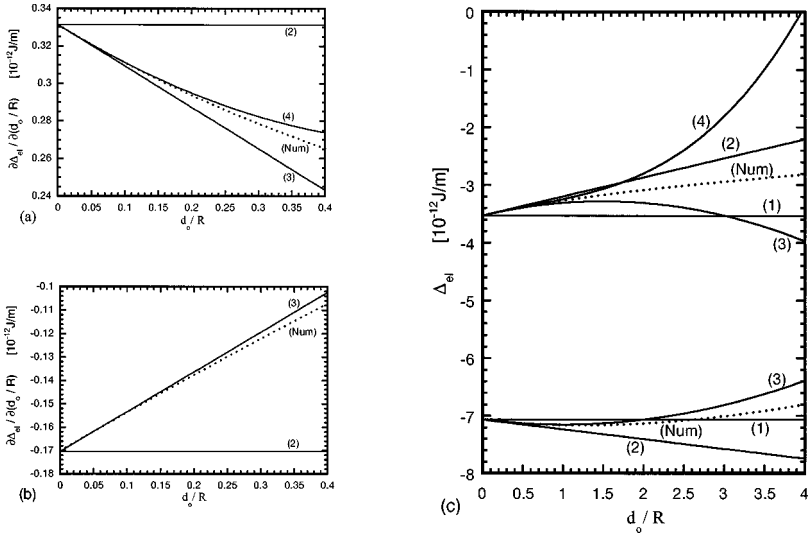

FIG. 6. The analog of Fig. 5 for one surface charge per 67 Å^2, with d_0 maintained at 50 Å.

the change from κ^{-1} to the common d_0 value throughout. The range for (a) and (b) now extends down to $R=2.5d_0=125$ Å and down to 12.5 Å in (c). The basic shapes of all curves in Figs. 5 and 6 are the same as those in Figs. 3 and 4, respectively. Again in parts (a) and (b) of Figs. 5 and 6 the accuracy of the approximations to the exact value of the second derivative improve uniformly with increasing order m, with the error growing on decreasing R to around 2–4 % at 125 Å for the highest orders considered in each case. In Figs. 5(c) and 6(c) the same pattern of wild deviations is apparent in the second half of the d_0/R range as the order of expansion is increased, especially so for the cylinder (the upper of the two curve sets). For the sphere, the straight line $(m=2)$ approximation in Fig. 5(c) and the constant $(m=1)$ for Fig. 6(c) both remain quite reasonable over the whole range displayed, but this is more by way of accident than true fit and will certainly not continue to smaller R as Δ_{el} tends to zero.

B. Padé approximants

Recall that in Sec. III we determined the electrostatic contribution to the elastic moduli of the curvature free energy expansion in Eqs. (1) and (2) by matching the coefficients of successive powers of $1/R$ in Δ_c for cylinders and spheres, Eq. (3), to those generated by the corresponding asymptotic expansion of Δ_{el} for the PB cell model in these two geometries. We have now seen, through the preceding four examples, that the resulting power series expansion is completely unsuitable as an approximation to the exact Δ_{el} for larger values of $1/R$. The only recourse in these circumstances seems to be a numerical evaluation of the free energy. However, we shall now describe a means of recasting the curvature expansion in Eq. (3) to extend its range of applicability. In particular, we focus on the technique of Padé approximants.

In this approach our function Δ_{el} is instead matched to a rational function in $1/R$; its (M,N) Padé approximant P_N^M is

$$P_N^M(R)=\frac{\sum_{k=0}^{M} a_k(1/R)^k}{\sum_{k=0}^{N} b_k(1/R)^k}. \tag{34}$$

We then proceed as before, demanding that the power series expansion of this given form in $1/R$ about the planar state agrees with that for Δ_{el}, i.e., that already derived by matching to Eq. (3) (which is just the special case $N=0$), up to and including the power $(1/R)^{M+N}$. This gives a system of linear equations for the $M+N+1$ independent coefficients a_k and b_k. For example, if the expansion in Eq. (3a) or (3b) is written as $\Sigma_{k=0}c_k(1/R)^k$ then the corresponding Padé approximant P_2^0 for cylinder or sphere is given by

$$P_2^0(R)=\frac{c_0}{1-(c_1/c_0)(1/R)+[(c_1/c_0)^2-c_2/c_0](1/R)^2}, \tag{35}$$

with that for P_1^0 obtained by removing the $(1/R)^2$ term from the denominator. Note that, since the Padé coefficients are given directly in terms of the c_k, and hence the electrostatic contribution to the elastic moduli, we are still using the same curvature information, but now in a different manner.

Note that in excess salt the Debye-Hückel formula (23) for weakly charged spheres has precisely the form of a (0,2) approximant in $1/R$, in which the denominator is a perfect square. Thus, inserting into Eq. (35) the coefficients from Eq. (3b) given by their forms in Eq. (22), this Padé approximant reconstructs the exact Δ_{el}. For cylinders in this linear limit, Δ_{el} in Eq. (24) is clearly not a rational function in $1/R$ [neither is the small R asymptotic form $-(\kappa R)^2\ln(\kappa R)$ of the braced part], however the approximants (0,1), (0,2), or (1,2) could still be useful.

We illustrate these Padé approximants using the same four examples as shown in Figs. 3–6. For the first example, with 250 mM salt in excess, Δ_{el} for the cylinder and sphere in Fig. 3(c) are replotted over the same range of κ^{-1}/R in Figs. 7(a) and 7(b) and compared to the approximants (0,1) and (1,2), and (0,2), respectively. These approximants, which are guaranteed to match the asymptotics at large R to order $(1/R)^{M+N}$, are no longer dominated by this power as R increases, and follow the exact curve over most or all of the range. For the cylinder in Fig. 7(a), even the simplest approximant (0,1) remains reasonably accurate, with its error rising in magnitude to around 5% as κ^{-1}/R approaches 2. The higher approximant (1,2), obtained by including the

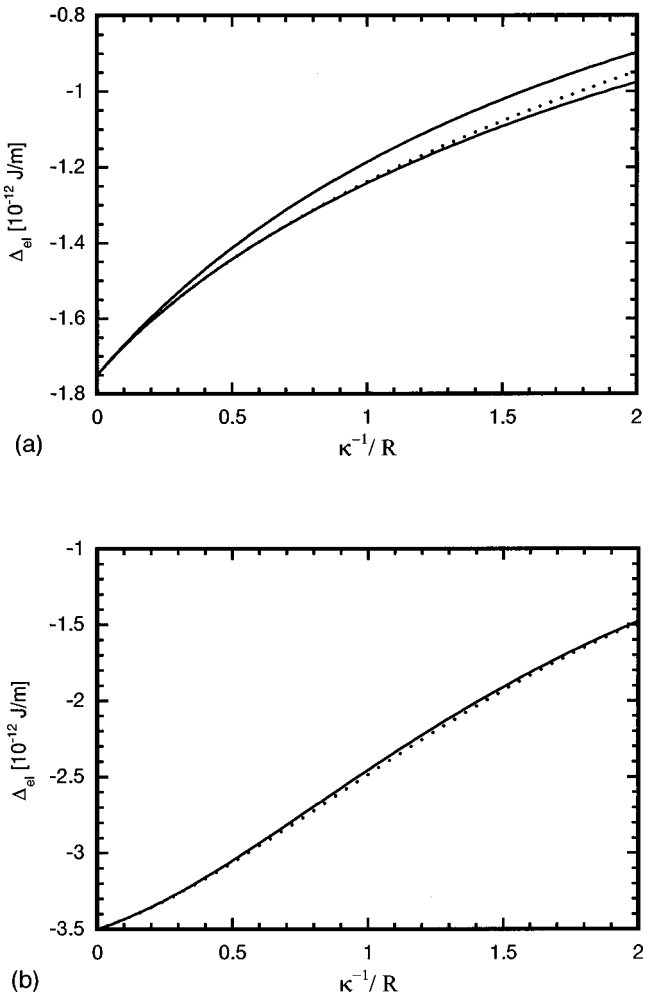

FIG. 7. PB cell models for 250 mM salt in excess and a surfactant headgroup area of 67 $Å^2$ (as for Fig. 3), now comparing the numerical solution (dotted) with the Padé approximants (a) (0,1) (upper) and (1,2) (lower) for the cylinder, and (b) (0,2) for the sphere.

fourth-order modulus [Eq. (A8)], is even better; the deviation is quite negligible for $\kappa^{-1}/R<1$ and increases to around 3% at the end point. For the spherical geometry in Fig. 7(b), the accuracy of the (0,2) approximant [Eq. (35)] is more impressive still in its ability to capture the inflection in Δ_{el}.

For the other three examples (Figs. 4–6) we shall briefly describe the Padé approximants rather than showing full pictures. In the second example, with 10 mM salt in excess, the exact Δ_{el} for the cylinder [in Fig. 4(c)] is also accurately approximated by the (1,2) form; the error again rises to around 3% at $\kappa^{-1}/R=2$. The (0,1) form has now lost accuracy and is more than 10% above the exact value at this end point, albeit a considerable improvement on the straight line ($m=2$) approximation which uses the same two curvature moduli $k_c H_0$ and k_c. For the spherical geometry the (0,2) form used in the first example ceases to be a good approximation here, since its justification above via the Debye-Hückel limit no longer applies to a sphere at such low screening. For the counterions-only example with the lower surface charge, the approximants (0,1) and (1,2) for the cylinder both follow closely the exact Δ_{el} [Fig. 5(c)] and deviate by less than 5% up to $d_0/R=4$. The (0,2) form is again the best choice for the sphere, and is accurate to around 10%. At the higher surface charge, the curve for the cylinder [the upper in Fig. 6(c)] is approximated within 1% by the (1,2) form, while the error approaches 10% using (0,1). Again, at such high charge the curve for the sphere [the lower in Fig. 6(c)] cannot be fitted accurately using the (0,2) approximant.

Although the cylindrical geometry with only counterions present is exactly solvable [Eqs. (27)–(29)] and so not directly in need of approximation, these four examples together illustrate the trends in the Padé approach. Since the approximants (M,N) either succeed or fail in both extremes ($\alpha_0=0$ and 1) over comparable regimes of surface potential (i.e., θ_0^s), this suggests that these same forms apply across the entire range $0<\alpha_0<1$ using the θ function developments of the moduli formulas at general composition [Eqs. (15)–(19)].

V. DISCUSSION AND CONCLUDING REMARKS

As stated at the outset, one main purpose of mapping the phenomenological bending energy approach to molecular quantities involves the practical matter of the analysis of experiments which either directly attempt to measure the bending moduli, or the interpretation of which relies on some understanding of how the moduli depend on experimental variables. There are numerous examples of both cases. A review of experimental work up to 1994 on measuring the bending constants, particularly in AOT [sodium bis(2-ethylhexyl) sulfosuccinate] systems, has been given by Kellay *et al.* [27]. Since then, Kegel *et al.* [28] have performed ellipsometric measurements of the bending rigidity of SDS (sodium dodecyl sulfate) systems, focusing mainly on the scaling of the moduli with addition of an alcohol cosurfactant. More recently, Eastoe *et al.* [29] have attempted to investigate specifically the electrostatic contribution to the bending moduli of *n*-alkyl-*n*-dodecyldimethylammonium bromide microemulsion droplets, using surface light scattering and small-angle neutron scattering. Their work is a good example of how the results we have presented herein can be of use. Eastoe *et al.* base their experimental analysis on the Mitchell-Ninham-Lekkerkerker [4,5] calculations of the bending moduli in excess salt (although we do not agree with some of their assumptions [30]). Since Eastoe *et al.* work over a range of salt concentrations, from zero to an excess of added salt, a unified treatment of their results requires the generalized formulas (15)–(17), for which the rapidly convergent series (in Appendixes A and B), bridging these two extremes, can be directly applied. Furthermore, the radii of the droplets are $\approx$20 Å, and especially for the low salt concentrations, the harmonic approximation will break down. A reinterpretation of these results in terms of the Padé scheme presented in Sec. IV B would then be more appropriate.

Another interesting development is the observation and prediction of ''microvesicles,'' formed by mixed ionic-nonionic surfactant systems with cosurfactant and water, by Oberdisse, Porte, and co-workers [31]. We concur with their assertion that these microvesicles are of too small radius for the harmonic truncation of the bending energy to be justified, therefore necessitating a numerical solution of the PB cell

model; we can suggest that the Padé approximants may also be of value. As a general statement, however, it is not the purpose of this paper to embark on a large-scale reinterpretation of existing experimental data, and we mean here only to give some indications of how our results may be utilized.

We reiterate that the aim of this study has been both to extend and to test the limits of applicability of the curvature description of ionic surfactant interfaces. The established dependence of the harmonic-order moduli on system parameters has now been extended to their anharmonic analogs. The determination of the range of applicability of the curvature expansion at these successive orders is especially important, given the scope for highly erroneous predictions outside these bounds. Also, we have investigated a Padé scheme, which permits a modified curvature description to function well as an approximation to the full free energy, even at large curvatures, and present it as an alternative to a purely numerical approach for dealing with highly curved aggregates. This approach may provide yet a further reason to persist with the highly successful curvature description of surfactant mesophases.

ACKNOWLEDGMENTS

We thank J. Ennis and B. W. Ninham for some very helpful suggestions. A.F. appreciates support from the Swedish Natural Science Research Council (NFR) for his visit to the Department of Applied Mathematics, Australian National University, and J.D. is grateful to the Australian Research Council for its support.

APPENDIX A: EXCESS SALT

In excess salt ($\alpha_0=1$) the Jacobi elliptic function for the planar potential ϕ_0 reduces to a hyperbolic. If we define the scaled distance $X=\kappa(r-R)$, where κ^{-1} is the Debye screening length in Eq. (20), then the solution in Eq. (9) now becomes

$$\phi_0=2\ln\{\tanh[(X+X_s)/2]\}. \tag{A1}$$

Here we have switched from the parameter θ_0^s to X_s, in terms of which Eq. (10) becomes

$$\coth X_s\equiv t_s=[1+(\kappa^{-1}/\lambda_{GC})^2]^{1/2}. \tag{A2}$$

Equations (15)–(17) then give

$$k_cH_0=\frac{\varepsilon}{2\pi(\beta e)^2}\ln[(t_s+1)/2], \tag{A3}$$

$$\overline{k_c}=-\frac{\varepsilon\kappa^{-1}}{\pi(\beta e)^2}\int_0^{\ln[(t_s+1)/2]}du\,\frac{u}{[\exp(u)-1]}, \tag{A4}$$

$$k_c=\frac{\varepsilon\kappa^{-1}}{2\pi(\beta e)^2}\frac{(t_s-1)(t_s+2)}{t_s(t_s+1)}, \tag{A5}$$

and Eqs. (18) and (19) become

$$\lambda_1=-\frac{\varepsilon\kappa^{-2}}{6\pi(\beta e)^2}\frac{(t_s-1)}{t_s^3(t_s+1)^2}(9t_s^4+15t_s^3+16t_s^2+24t_s+8) \tag{A6}$$

and

$$\lambda_2=\frac{\varepsilon\kappa^{-2}}{\pi(\beta e)^2}\left\{\int_{\ln[(t_s+1)/(t_s-1)]}^{\infty}du\,\frac{u}{[\exp(u)-1]}+\left[\frac{2(t_s+2)}{t_s(t_s+1)}-\ln\left(\frac{t_s+1}{t_s-1}\right)\right]\ln\left(\frac{t_s+1}{2}\right)\right\}. \tag{A7}$$

The corresponding formula for the fourth-order modulus κ_1 was shown in a previous study [15] to be

$$\kappa_1=\frac{\varepsilon\kappa^{-3}}{192\pi(\beta e)^2}\frac{(t_s-1)}{t_s^5(t_s+1)^3}(53t_s^7+140t_s^6+155t_s^5+88t_s^4+64t_s^3+136t_s^2+96t_s+24). \tag{A8}$$

We now turn to analyzing the bending moduli at general system composition, in Eqs. (15)–(19). Expressing Eqs. (9) and (10) in terms of θ functions [24], the expansions of the general formulas about the excess-salt limit are extremely rapidly convergent; even the lowest-order corrections to Eqs. (A1)–(A8) remain highly accurate approximations far away from this limit. Relabeling the modulus of the elliptic integral in Eq. (9) as $k\equiv\alpha_0^{1/2}=(n^c_{-,0}/n^c_{+,0})^{1/2}$, its complementary nome q' is given by

$$q'=\Delta'(1+2\Delta'^4+15\Delta'^8+150\Delta'^{12}+\cdots), \tag{A9a}$$

where

$$\Delta'=\frac{1}{2}\left(\frac{1-k^{1/2}}{1+k^{1/2}}\right). \tag{A9b}$$

We develop about the limit $k=1$ in ascending powers of q'; in all subsequent equations the terms omitted are of order q'^4.

By analogy with Eq. (20) we introduce the scaling length κ_p^{-1}, given in terms of the general λ_D in Eq. (7) as

$$\kappa_p^{-1}=\frac{1}{2}(1+2q'+\cdots)^2\lambda_D. \tag{A10}$$

Using the charged boundary condition, phrased in Eq. (10), it is convenient to define the auxiliary parameter t_p [generalizing t_s in Eq. (A2)],

$$t_p=[1+(\kappa_p^{-1}/\lambda_{GC})^2+8q'^2]^{1/2}+\cdots. \tag{A11}$$

The expansions of Eqs. (15)–(17) in terms of q' and t_p then become

$$k_cH_0=\frac{\varepsilon}{2\pi(\beta e)^2}\{\ln[(t_p+1)/2]-q'^2(A^2+2)+\cdots\}, \tag{A12}$$

$$\overline{k_c}=-\frac{\varepsilon\kappa_p^{-1}}{\pi(\beta e)^2}\left[\int_0^{\ln[(t_p+1)/2]}du\,\frac{u}{[\exp(u)-1]}+q'^2(A^3/3+2A)+\cdots\right], \tag{A13}$$

and

$$k_c=\frac{\varepsilon\kappa_p^{-1}}{2\pi(\beta e)^2}\left(\frac{(t_p-1)(t_p+2)}{t_p(t_p+1)}+q'^2\left\{\left(\frac{t_p-1}{t_p+1}\right)^2-8\left(\frac{t_p-1}{t_p+1}\right)-2A^2+2A\left[\frac{8}{t_p(t_p+1)}-2\left(\frac{t_p-1}{t_p+1}\right)-1\right]\right\}+\cdots\right), \tag{A14}$$

where we have used the abbreviation

$$A=\ln\left[q'^2\left(\frac{t_p+1}{t_p-1}\right)\right]. \tag{A15}$$

Corresponding expansions for the third-order moduli in Eqs. (18) and (19) can be derived by following this same prescription.

APPENDIX B: COUNTERIONS ONLY

In the absence of added salt (i.e., $\alpha_0=0$), the Jacobi elliptic function for ϕ_0 degenerates to a simple trigonometric, and Eq. (9) becomes

$$\phi_0=2\ln[\cos(D_0-x)]. \tag{B1}$$

The additional relation (10) specifying the length λ_D, through $D_0=d_0/\lambda_D$, in terms of the ratio d_0/λ_{GC} is then

$$D_0\tan D_0=d_0/\lambda_{GC}. \tag{B2}$$

Equations (15)–(17) simplify to

$$k_cH_0=-\frac{\varepsilon}{4\pi(\beta e)^2}[2\ln(\cos D_0)+D_0^2], \tag{B3}$$

$$\overline{k_c}=\frac{\varepsilon d_0}{\pi(\beta e)^2}\left[\frac{2}{D_0}\int_0^{D_0}dt\,\ln(\cos t)+\frac{1}{3}D_0^2\right], \tag{B4}$$

$$k_c=-\frac{\varepsilon d_0}{2\pi(\beta e)^2}\left[2\cos 2D_0-\frac{(1-D_0^2)}{D_0}\sin 2D_0+\frac{2}{3}D_0^2\right]. \tag{B5}$$

Equations (18) and (19) give the following formulas for the third-order moduli:

$$\lambda_1=\frac{\varepsilon d_0^2}{6\pi(\beta e)^2}\frac{1}{D_0^2}\{(1+3D_0^2)\cos 4D_0+2D_0^3\sin 4D_0-4(1-6D_0^2)\cos 2D_0-4D_0(3-4D_0^2)\sin 2D_0+(3-3D_0^2+8D_0^4)\}, \tag{B6}$$

$$\lambda_2=-\frac{\varepsilon d_0^2}{\pi(\beta e)^2}\frac{1}{D_0^2}\left\{4\int_0^{D_0}dt\,t\ln(\cos t)+2(\cos 2D_0+D_0\sin 2D_0+1)\ln(\cos D_0)+D_0^2\cos 2D_0+D_0^3\sin 2D_0+\left(D_0^2+\frac{5}{6}D_0^4\right)\right\}. \tag{B7}$$

Equations (B3), (B5), and (B6) have also been verified by using the exact solution for the cylindrical cell model with counterions only, in Eqs. (27)–(29), and performing the expansion in λ_D/R described in the main text. Continuing this expansion up to $(\lambda_D/R)^3$ we obtain the following formula for the modulus κ_1 associated with the free energy cost at fourth order in mean curvature [see Eq. (21)]:

$$\kappa_1=-\frac{\varepsilon d_0^3}{32\pi(\beta e)^2}\frac{1}{D_0^3}\left\{\frac{1}{3}(2D_0+D_0^3)\cos 6D_0-\frac{1}{6}(1-3D_0^2-2D_0^4)\sin 6D_0+2(2D_0+D_0^3)\cos 4D_0-(1-4D_0^2-3D_0^4)\sin 4D_0-\left(6D_0-\frac{71}{3}D_0^3\right)\cos 2D_0+\frac{1}{2}\left(1-27D_0^2+\frac{106}{3}D_0^4\right)\sin 2D_0+\left(\frac{16}{3}D_0-2D_0^3+\frac{36}{5}D_0^5\right)\right\}. \tag{B8}$$

Note that Eqs. (B5)–(B8) all pertain to the constraint of fixing the counterion chemical potential on bending.

To partner Eqs. (A9)–(A15), we provide the analogous θ function expansions of the general moduli formulas about this opposing extreme of counterions only. We now develop from $k=0$ in ascending powers of the nome q, which is given by Eq. (A9) with the primes removed and k switched to its complementary modulus $k'=(1-k^2)^{1/2}$. The terms omitted in the expansions below are of order q^3.

The auxiliary parameter is labeled z_0 [for comparison with D_0 in Eq. (B2)] and, from the charged boundary condition, is the solution of

$$z_0(\tan z_0-4q\sin 2z_0+8q^2\cos z_0\sin 3z_0+\cdots)=d_0/\lambda_{GC} \tag{B9}$$

in the range from 0 to $\pi/2$. The expansions of Eqs. (15)–(17) are then given by

$$k_cH_0=-\frac{\varepsilon}{4\pi(\beta e)^2}\{[2\ln(\cos z_0)+z_0^2]+8q(z_0^2-\sin^2 z_0)-8q^2(z_0^2-\sin^2 z_0\cos 2z_0)+\cdots\}, \tag{B10}$$

$$\overline{k_c}=\frac{\varepsilon d_0}{\pi(\beta e)^2}\left\{\left[\frac{2}{z_0}\int_0^{z_0}dt\ \ln(\cos t)+\frac{1}{3}z_0^2\right]-2q\left(2-\frac{4}{3}z_0^2-\frac{\sin 2z_0}{z_0}\right)-2q^2\left(1+\frac{4}{3}z_0^2-\frac{\sin 2z_0}{z_0}+\frac{1}{4}\frac{\sin 4z_0}{z_0}\right)+\cdots\right\}, \tag{B11}$$

and

$$k_c=-\frac{\varepsilon d_0}{2\pi(\beta e)^2}\left\{\left(\frac{2}{3}z_0^2+2P_{1,1}\right)+8q\left[\frac{10}{3}z_0^2+z_0\sin 2z_0+4P_{1,1}(\cos^4 z_0+\cos^2 z_0+2)\right]-32q^2\left[2\left(3-\frac{29}{4}z_0^2\right)+\left(9+\frac{13}{4}z_0^2\right)\frac{\sin 2z_0}{z_0}-2P_{1,1}(8\cos^6 z_0+1)\cos^2 z_0-P_{3,5}(\cos^4 z_0+\cos^2 z_0+2)\right]+\cdots\right\}, \tag{B12}$$

where

$$P_{m,n}=mn\cos 2z_0-\frac{1}{2}(m^2-n^2z_0^2)\frac{\sin 2z_0}{z_0}. \tag{B13}$$

[1] W. Helfrich, Z. Naturforsch. C **28**, 693 (1973).
[2] M. Winterhalter and W. Helfrich, J. Phys. Chem. **92**, 6865 (1988); **96**, 327 (1992).
[3] B. Duplantier, R. E. Goldstein, V. Romero-Rochín, and A. I. Pesci, Phys. Rev. Lett. **65**, 508 (1990).
[4] D. J. Mitchell and B. W. Ninham, Langmuir **5**, 1121 (1989).
[5] H. N. W. Lekkerkerker, Physica A **159**, 319 (1989); **167**, 384 (1990).
[6] A. Fogden, D. J. Mitchell, and B. W. Ninham, Langmuir **6**, 159 (1990); A. Fogden and B. W. Ninham, *ibid.* **7**, 590 (1991).
[7] P. Pincus, J.-F. Joanny, and D. Andelman, Europhys. Lett. **11**, 763 (1990); P. G. Higgs and J.-F. Joanny, J. Phys. (Paris) **51**, 2307 (1990); J. L. Harden, C. Marques, J.-F. Joanny, and D. Andelman, Langmuir **8**, 1170 (1992).
[8] I. Szleifer, D. Kramer, A. Ben-Shaul, D. Roux, and W. M. Gelbart, Phys. Rev. Lett. **60**, 1966 (1988); I. Szleifer, A. Ben-Shaul, and W. M. Gelbart, J. Phys. Chem. **94**, 5081 (1990); I. Szleifer, D. Kramer, A. Ben-Shaul, W. M. Gelbart, and S. A. Safran, J. Chem. Phys. **92**, 6800 (1990).
[9] J. Ennis, J. Chem. Phys. **97**, 663 (1992).
[10] D. M. McAvity, J. Phys. A **26**, 823 (1993).
[11] R. de Vries, J. Chem. Phys. **103**, 6740 (1995).
[12] G. Porte and C. Ligoure, J. Chem. Phys. **102**, 4290 (1995).
[13] J. Daicic, A. Fogden, I. Carlsson, H. Wennerström, and B. Jönsson, Phys. Rev. E **54**, 3984 (1996).
[14] A. Fogden, J. Daicic, D. J. Mitchell, and B. W. Ninham, Physica A **234**, 167 (1996).
[15] A. Fogden, J. Daicic, and A. Kidane, J. Phys. II **7**, 229 (1997).
[16] A. Fogden and J. Daicic, Colloids Surf. A **129–130**, 157 (1997).
[17] D. Andelman, in *Handbook of Biological Physics*, edited by R. Lipowsky and E. Sackmann (Elsevier, Amsterdam, 1995), Chap. 12.
[18] R. Bruinsma, J. Phys. II **2**, 425 (1992).
[19] H. Wennerström and U. Olsson, Langmuir **9**, 365 (1993); J. Daicic, U. Olsson, H. Wennerström, G. Jerke, and P. Schurtenberger, J. Phys. II **5**, 199 (1995); J. Daicic, U. Olsson, and H. Wennerström, Langmuir **11**, 2451 (1995).
[20] M. D. Mitov, C. R. Acad. Bulg. Sci. **31**, 513 (1978).
[21] D. C. Morse, Curr. Opin. Colloid Interface Sci. **2**, 365 (1997).
[22] Note that our definitions of the coupling constants λ_1, λ_2, λ_3 correspond, respectively, to multiples of 8, 2, 2 of the ones in Mitov's paper.
[23] In fact, since our perturbative approach does not make explicit use of the planar solution, the generality of these moduli formulas could well be extended to potentials beyond the simple Poisson-Boltzmann description.
[24] E. T. Whittaker and G. N. Watson, *A Course of Modern Analysis* (Cambridge University Press, Cambridge, England, 1996).
[25] B. W. Ninham and V. A. Parsegian, J. Theor. Biol. **31**, 405 (1971).
[26] J. Liouville, J. Math. Z **18**, 71 (1853).
[27] H. Kellay, B. P. Binks, Y. Hendrikx, L. T. Lee, and J. Meunier, Adv. Colloid Interface Sci. **49**, 85 (1994).
[28] W. K. Kegel, I. Bodnàr, and H. N. W. Lekkerkerker, J. Phys. Chem. **99**, 3272 (1995).
[29] J. Eastoe, D. Sharpe, R. K. Heenan, and S. Egelhaaf, J. Phys. Chem. B **101**, 994 (1997).
[30] Unfortunately, we cannot agree with the interpretation of Eastoe *et al.* [29] that the theories of Mitchell and Ninham [4] and Lekkerkerker [5] give different results for the bending moduli; their results are in fact identical, if the specification is made as to whether a charged bilayer [4] or monolayer [5] is being considered. The interpretation of the bilayer thickness t appearing in the Mitchell-Ninham result for $\overline{k_c}$ as being suitable for the interfacial thickness in a monolayer phase, as in Ref. [29], is incorrect, as t only enters when the bending of two juxtaposed charged surfaces is under consideration, as in the case of a bilayer. Also, we feel that the use of these excess-salt results is inappropriate for the samples with low concentrations of added electrolyte, certainly those where no salt was added.
[31] J. Oberdisse, C. Couve, J. Appell, J. F. Berret, C. Ligoure, and G. Porte, Langmuir **12**, 1212 (1996); J. Oberdisse and G. Porte, Phys. Rev. E **56**, 1965 (1997).